

Optical Enhancement of Blending Reduced Graphene Oxide with Poly(vinyl alcohol) Nanocomposite

Mohammed Fadhil¹, Hadia H. Naseef^{*1}, Riad M. Hameed², Ali Sabah Hussein³

¹Department of Physics, College of Science, Mustansiriyah University, 10052 Baghdad, IRAQ, ²General Administration of Education, Rusafa II, Ministry of Education, Baghdad, IRAQ, ³Department of Applied Science, University of Technology, Baghdad, IRAQ.

Abstract

In this study, we present findings on the optical, structural, and dielectric properties of reduced graphene oxide (rGO)-doped poly(vinyl alcohol) (PVA) nanocomposites. The novelty of this work lies in the comprehensive investigation of optical transparency and band structure parameters across various rGO nanosheet concentrations within the PVA polymer. Several techniques are employed to examine the morphological, structural, and optical properties of the prepared nanocomposites including scanning electron microscopy (SEM), Raman spectroscopy, Fourier-transform infrared spectroscopy (FTIR), and UV-visible spectroscopy. The optical bandgap of the nanocomposites was determined, in addition to the refractive index, optical dielectric constants, and optical conductivity of pure rGO, pure PVA, and rGO-doped PVA nanocomposites. SEM analysis presented detailed imaging of the morphological structure of the nanocomposites. Raman spectroscopy exhibited a decrease in D-band intensity accompanied by an increase in crystalline size, and a decrease in G-band intensity with a lower $I_{D/G}$, revealing a variation in crystalline size from 35.33 nm to 12.24 nm. The dielectric constant verified an increase with the rise in rGO content at a particular frequency. Understanding the mechanisms underlying the optical properties of rGO-doped PVA nanocomposites could suggestively advance the expansion of more efficient and cost-effective materials for many optical applications. As research progresses, these nanocomposites are prospective to play an essential role in the advancement of technologies such as flexible electronics, smart sensors, and next-generation photonic devices.

Keyword: reduced graphene oxide • optical enhancement • poly(vinyl alcohol) • nanocomposite • energy band.

Introduction

Reduced Graphene Oxide (rGO) is a result of oxygen removal from graphene oxide and has gained substantial consideration across various domains due to its owing features, such as high electrical conductivity, and a large surface area [1, 2]. These properties make the rGO as most desirable material for electronics, energy storage, and sensor applications. The reduction or elimination of the oxygen process from graphene oxide, rallies the electronic properties of rGO, making it an adaptable component for composite materials [3, 4].

Poly(vinyl alcohol) (PVA) is a synthetic polymer identified for its solubility in H₂O and organic solvents, biocompatibility, and stability as films [5]. PVA is commonly utilized in pharmaceuticals, food processing, and as a stabilizing agent in various chemical processes. Its adaptability and capability to form hydrogen bonds with other molecules make PVA an ideal applicant for producing composite materials with enhanced properties [6].

***Address for correspondence:** Dr. Hadia H. Naseef, Department of Physics, College of Science, Mustansiriyah University, Baghdad 10052, Iraq.

E-mail: hadia.hatim@uomustansiriyah.edu.iq

ORCID: <https://orcid.org/0009-0007-5239-651X>

This is an open access journal, and articles are distributed under the terms of the Creative Commons Attribution License (CC-BY-NC) 4.0 License, which allows others to use, distribution, and reproduction in any medium for noncommercial purposes, as long as the original work is cited properly.

Info:

Submitted: 12 Nov. 2024;

Revised: 05 Jan. 2025;

Accepted: 26 Jan. 2025;

Published: 10 Feb. 2025.

<https://doi.org/10.71109/nmi.2025.1.1.10>

Merging rGO with PVA results in a composite material that yields the unique properties of both components [7]. rGO-doped PVA composites determine upgraded mechanical strength, thermal stability, and electrical conductivity [8]. Of particular attention are the optical parameters of these composites, which are valued for applications in optoelectronics, sensors, and photodetectors. The interaction between rGO and PVA can chief significant improvements in optical characteristics and light absorption, making such composites promising materials for advanced applications [6, 9].

In this research, the optical parameters enhancements in rGO-doped PVA composites were observed, attributable to the effects of high electron mobility of rGO and PVA's stabilizing matrix. This improvement not only widens the potential applications for these materials but also opens new paths for research in material science. Understanding the mechanisms of rGO-doped PVA nanocomposites optical properties can lead to the synthesis of more efficient and cost-effective nanocomposites for use in a varied range of optical devices. As research advances, rGO-doped PVA nanocomposites could play a central role in the development of technologies such as flexible electronics, smart sensors, and next-generation photonic devices.

Experimental Part

Graphite rod was exfoliated under optimization conditions according to our previous literature to synthesize high purity and low oxygen ratio of rGO nanosheets [3, 4]. In order to prepare rGO-PVA nanocomposite films with various concentrations, rGO and PVA powders were dispersed in 100 ml of DI water and ultrasonically dissolved with several



concentrations of 0.125, 0.25, 0.5, 0.75, and 1.0 wt%, labeled as PVA (without rGO), PG1, PG2, PG3, PG4, and PG5, rGO (without PVA), respectively.

The ideal fixation of weight percentage was quantified using the equation^[10]:

$$wt\% = [w_G / (w_P + w_G)] \times 100 \quad \dots (1)$$

where rGO weight is (w_G) and (w_P) is the PVA is the weight.

0.20 μl of each mixture were dropped on a glass slide as a substrate, then after, the samples were dried at 40°C, a TESCAN MIRA 3 scanning electron microscope (SEM) was used to investigate the morphology resulting in rGO nanosheets and the mixture rGO–PVA. Moreover, the samples were characterized by a T70/T80 Series UV-Vis-Near IR spectrometer. Furthermore, to locate the bands of each film, Raman spectroscopy (Via TM Renishaw, UK) and identification of functional groups FTIR (Biotech Engineering Management) were engaged.

Results and Discussion

Figure 1a displays the surface morphology of rGO, while, **Figure 1b** exhibits the magnified located area of Figure 1a, the rGO nanosheet was folded and has a very thin texture. **Figure 1c** illustrates the upper morphology of the rGO-doped PVA sample. The SEM image reveals a sponge-like surface with well-distributed exfoliated rGO nanosheets within the PVA matrix.

Raman spectroscopy is an excellent technique for probing the underlying properties of materials, especially carbonaceous ones^[3,4]. **Figure 2a** shows the Raman spectra for pure rGO, pure PVA, and rGO-doped PVA (sample PG5) within the wavenumber range of 600 to 1800 cm^{-1} . For the rGO sample, two prominent bands appear at 1327 cm^{-1} and 1575 cm^{-1} , corresponding to the characteristic D and G bands, respectively^[4].

The D band is indicative of defects or the breakdown of rGO nanosheets, primarily related to the edges of the nanosheets. This band, observed at the lower wavenumber, arises from the breathing mode of A_{1g} symmetry k-phonons, which are activated by defects in the graphene structure^[11]. The G band, on the other hand, is associated with the first-order scattering of the E_{2g} vibration mode originating from the in-plane vibration of sp^2 carbon atoms^[12]. In the PVA spectrum, a weak peak at 1440 cm^{-1} is attributed to the bending of CH and OH groups^[13]. The rGO comprises graphene layers with residual oxygen groups attached to the planes and edges^[14]. The overall intensity ratio of the D band to the G band (I_D/I_G) provides insight into the degree of disorder in the graphitic material^[15].

The Raman spectra of rGO-doped PVA show intense D and G bands, confirming the presence of defects in the graphene layers. The I_D/I_G ratio changes in the rGO-doped PVA compared to pure rGO, likely due to the disruption of hydrogen bonding in the PVA hydroxyl groups and increased CH- π interactions between rGO and PVA^[16]. The characteristic D and G peaks also indicate the successful integration of rGO into the PVA matrix.

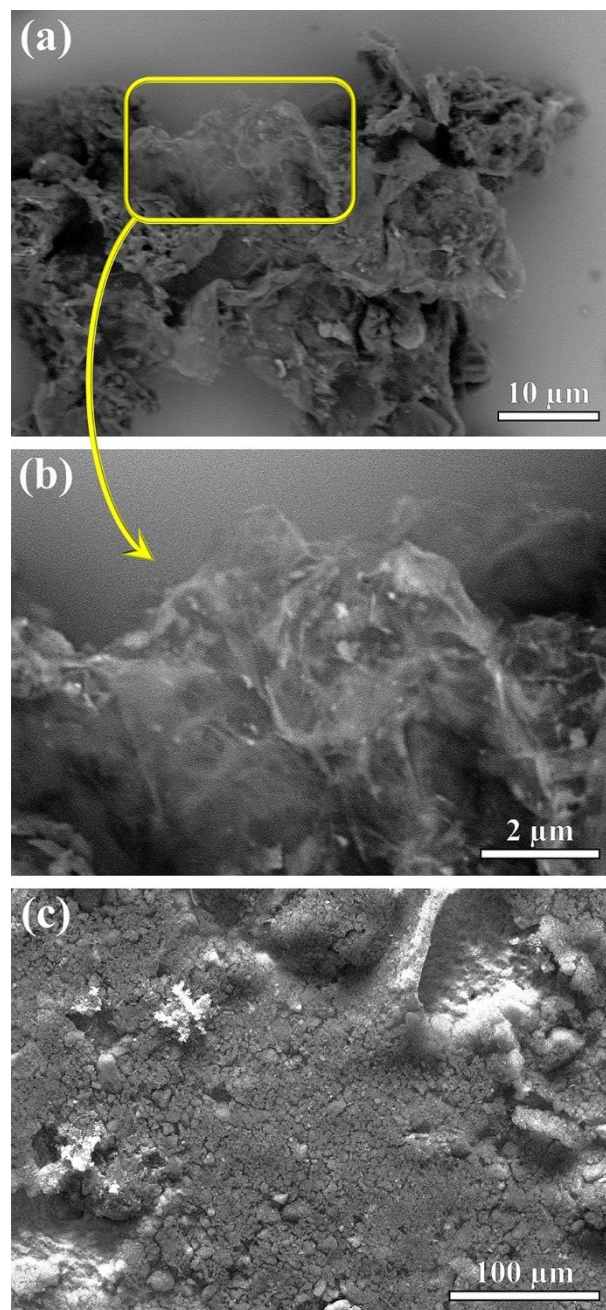


Figure 1. SEM micrograph of (a) rGO nanosheet, (b) magnified the located area of (a), and (c) RGO-doped PVA film.

The Raman region between 1132 and 1785 cm^{-1} for rGO and rGO-doped PVA was deconvoluted into G and D peaks using Gaussian functions. The full width at half maximum (FWHM or β) for the G and D peaks in pure rGO were found to be 69.2 cm^{-1} and 71.1 cm^{-1} , respectively. In contrast, the FWHM values for the G and D peaks in rGO-doped PVA were 97.3 cm^{-1} and 112 cm^{-1} , respectively. The higher β values in the rGO-doped PVA suggest a greater number of defects, which may be attributed to higher oxygen content.

This discrepancy could be due to variations in oxygen content or differences in the degree of exfoliation and crystalline size (L_a). The average size of adjacent carbon atoms in the rGO and rGO-doped PVA samples was estimated using the Tuinstra–Koenig relationship^[17, 18]:

$$L_a = (2.4 \times 10^{-10}) \times \left(\frac{I_G}{I_D}\right) \times \lambda^4 \quad \dots (2)$$

where λ is the laser wavelength, I_D and I_G are the Raman peak intensities of D and G peaks, respectively.

Remarkably, we observed a changing trend of L_a values from 35.33 to 12.24 nm from rGO to rGO-doped PVA samples.

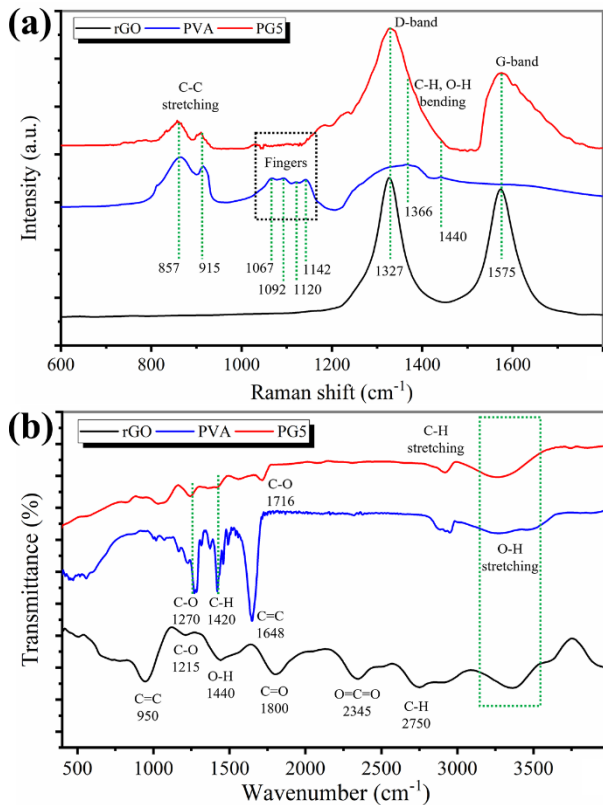


Figure 2. (a) Raman spectrum of rGO, PVA, and rGO-doped PVA, (b) FTIR spectrum of rGO, PVA, and rGO-doped PVA.

The performance of the rGO-doped PVA nanocomposite can be significantly enhanced through robust interactions at the nanofiller-polymer matrix interface. It is well-established that O-H and C-H stretching vibrations play a crucial role in hydrogen bond formation and interfacial interactions [19]. To evaluate the interaction between the nanofiller and the polymer, the samples' spectra were recorded and analyzed.

Figure 2b shows the FTIR spectra of pure rGO, pure PVA, and rGO-doped PVA samples. A broad absorption peak between 3200 and 3500 cm^{-1} indicates O-H symmetrical stretching, revealing the presence of strong intermolecular hydrogen bonding [20]. The absorption peaks at 1420, 2750, and 2923 cm^{-1} correspond to C-H stretching vibrations. The absorption peak at 1270 cm^{-1} in pure PVA, ascribed to the stretching vibrations of the C-O group [21], vanishes when rGO nanosheets are injected. The O-H stretching vibration peak at 3276 cm^{-1} in rGO-doped PVA shifts to a lower value of wavenumbers upon the integration of rGO nanosheets into the PVA matrix. This peak shift is attendant with the development of hydrogen bonds between the PVA chains and rGO nanosheets, which is expected due to the disruption of hydrogen bonding within the PVA hydroxyl groups [22, 23]. More additive of rGO nanosheets reduces the hydrogen bonding in the O-H groups of the PVA matrix, further shifting the peak to a lower value of wavenumbers. This reduction in

hydrogen bonding within the O-H groups of PVA enables the establishment of new hydrogen bonds between the PVA matrix and rGO nanosheets, improving the properties of the rGO-doped PVA nanocomposite [24].

The optical properties of the fabricated rGO, PVA, and rGO-doped PVA thin films were examined using UV-vis spectroscopy. The spectra were recorded over a wavelength range of 200 to 800 nm. **Figure 3** illustrates the UV-visible absorption and transmittance spectrum for pure rGO, pure PVA, and various weight percentages of rGO-doped PVA (PG1, PG2, PG3, PG4, and PG5). Pure PVA exhibits a prominent absorption peak at 226 nm, primarily caused by the carbonyl group within the PVA polymer, corresponding to the $\pi \rightarrow \pi^*$ transition [25]. In contrast, the highest absorption regions for rGO nanosheets and rGO-doped PVA samples are observed at wavelengths below 300 nm. The absorbance intensity of the rGO-doped PVA samples increases to levels comparable to that of the rGO nanosheets. This enhancement in absorbance is attributed to the strong interaction between the rGO nanosheets and the PVA polymer chains, which leads to the formation of robust bonding.

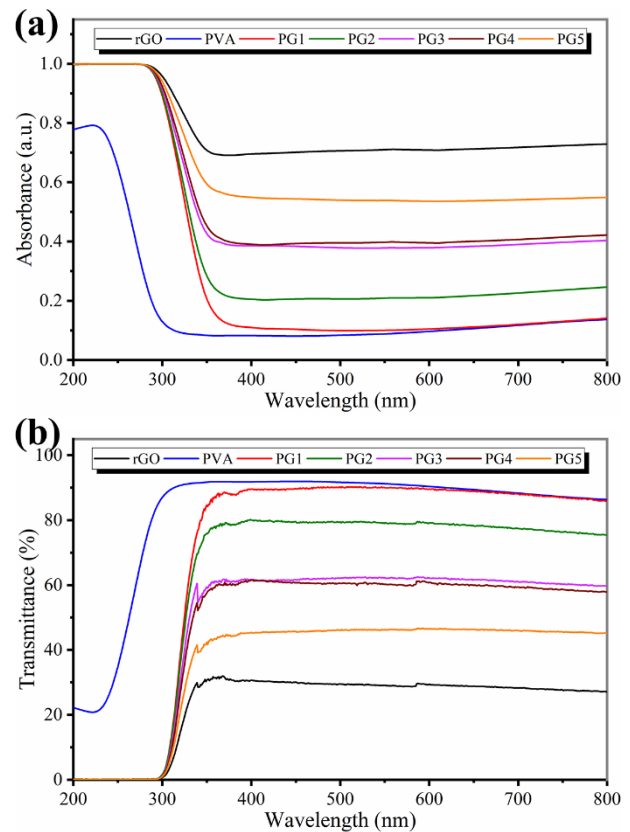


Figure 3. Absorbance (a) and Transmittance (b) spectrum for rGO, PVA, and PG1-PG5 nanocomposite samples.

The optical bandgap (E_g) of the rGO nanosheets, PVA, and PG1-PG5 nanocomposite samples was calculated using the Tauc plot method, assuming a direct bandgap for all samples. The variation of $(\alpha h\nu)^2$ versus the photon energy ($h\nu$) for rGO, PVA, and PG1-PG5 nanocomposite samples is shown in **Figures 4a-4g**. The direct bandgap values of the PVA polymer and rGO nanosheets exhibit significant differences, aligning well with previously published research [6, 26]. The E_g values decrease as the concentration of rGO nanosheets in the PVA polymer increases. This reduction in the bandgap is

attributed to the conducting nature of rGO nanosheets, which facilitates appreciable interfacial charge distribution and

enhances the conduction process within the rGO-doped PVA composites.

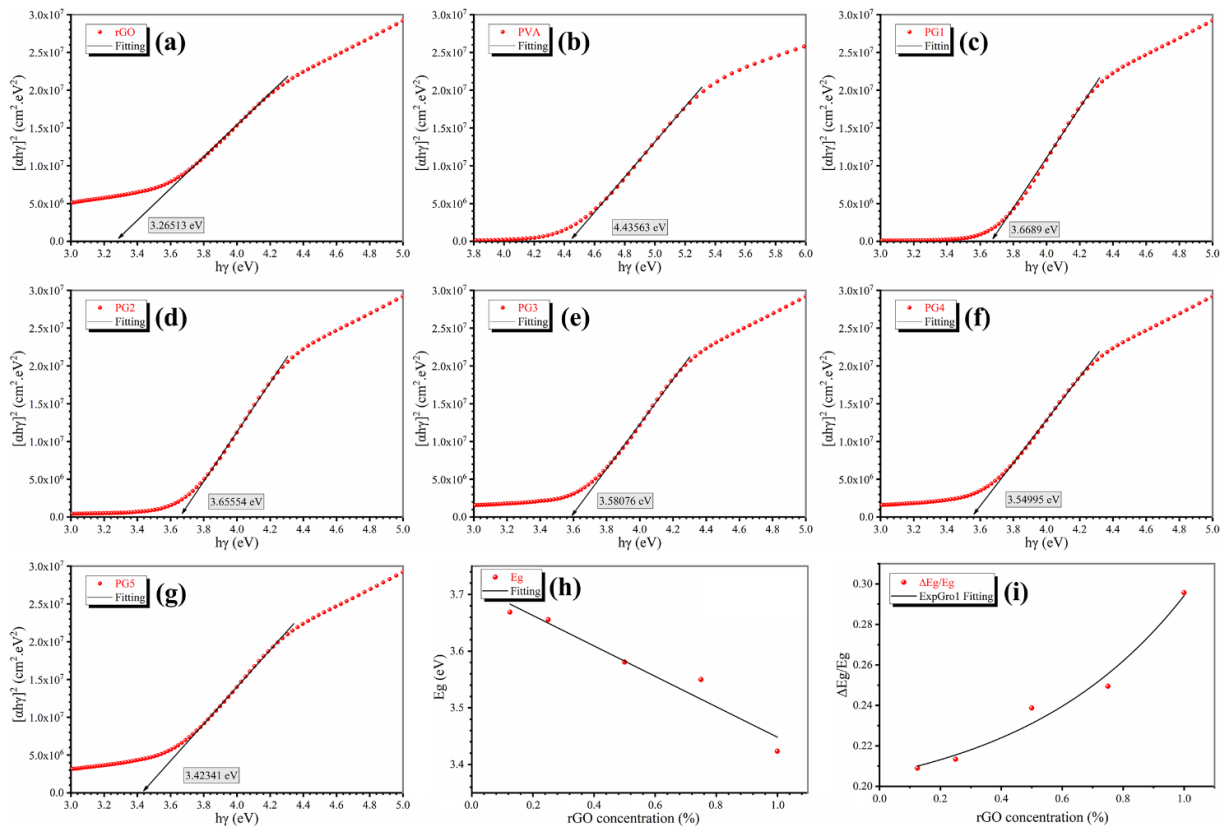


Figure 4. Tauc plots of direct optical bandgap estimation, (a) rGO nanosheets, (b) PVA polymer, (c) PG1 sample, (d) PG2 sample, (e) PG3 sample, (f) PG4 sample, and (g) PG5 sample, (h) linear relationship of E_g *vs.* rGO concentrations, (i) Plots of $\Delta E_g/E_g$ *vs.* rGO concentrations for the experimental results.

The linear relationship of E_g values change as a function of the rGO nanosheet concentration is demonstrated in **Figure 4h**, the linear fitting shows a well coefficient of determination as 0.92. To establish a universal analysis, we normalized the corresponding correlations with direct optical bandgap change are shown in **Figure 4i**. With the increase of rGO nanosheet concentrations, $\Delta E_g/E_g$ presents a growth feature that could be interpreted by a single-exponential model. Using the equation $\Delta E_g/E_g = Ae^{z/\tau}$, where A is the constant and z is the rGO nanosheets concentrations, to fit the curves, growth constants (τ) for the experimental results are 0.55072 ± 0.021 .

The investigation of the refractive index (n) and the extinction coefficient (k) is crucial for understanding the optical properties of materials. The extinction coefficient is essential for determining optical losses in a system [27]. The refractive index of pure rGO, pure PVA, and rGO-doped PVA nanocomposites (PG1-PG5) was studied using the equation [28, 29].

$$n = \frac{(1 + R)}{(1 - R)} + \sqrt{\left[\frac{4R}{(1 - R)^2} \right] - k^2} \quad \dots (3)$$

where reflectance (R) = $1 - (A + T)$ with A being absorbance and T being transmittance. The graphical plots of n and k as functions of wavelength (λ) for the investigated samples are shown in **Figures 5a** and **5b**, respectively. The

range of n and k values varies with wavelength from 1.1 to 4.2 and 0.4 to 7.2, respectively.

The optical conductivity (σ) of the fabricated materials was studied using the equation [30]:

$$\sigma = \frac{n\alpha c}{4\pi} \quad \dots (4)$$

where c is the speed of light (2.998×10^8 m/sec), and α is the absorption coefficient.

The optical conductivity for pure rGO nanosheets, pure PVA polymer, and the PG1-PG5 nanocomposites spans from 4×10^7 to 7×10^{10} S.cm⁻¹. **Figure 5c** illustrates how σ varies with wavelength. The real and imaginary parts of the optical dielectric constant (ϵ_r and ϵ_i) were also investigated through optical spectroscopy, providing insight into the overall band structure of rGO and rGO-doped PVA nanocomposites. The optical refractive index and dielectric constants are crucial parameters for characterizing the material's optical properties. The calculated values of n and k were used to derive ϵ_r and ϵ_i , as outlined in the following relations [30]:

$$\epsilon_r = n^2 - k^2 \quad \dots (5)$$

$$\epsilon_i = 2nk \quad \dots (6)$$

Figures 5d and **5e** depict the variations of ϵ_r and ϵ_i with wavelength for pure rGO nanosheets, pure PVA polymer, and the PG1-PG5 nanocomposites. The real part of the optical dielectric constant, which is linked to the optical refractive

index, significantly influences the propagation of electromagnetic waves through the material. The changes in ϵ_r and ϵ_i with varying compositions of rGO nanosheets can be attributed to the homogeneous dispersion of rGO nanosheets in the PVA polymer matrix and strong interfacial interactions between them.

The loss tangent ($\tan\delta$), influenced by the rGO nanosheets concentration and lattice strain, was determined using the equation [30, 31]:

$$\tan \delta = \epsilon_i / \epsilon_r \quad \dots (7)$$

The variation of the loss tangent with wavelength is illustrated in **Figure 5f**. The wavelength dependence of the loss tangent for rGO-doped PVA nanocomposites with different rGO concentrations reveals a unique behavior, with the highest peak at 235 nm decreasing as the rGO nanosheet concentration increases. This behavior may be related to the opposing trends in the loss tangent for rGO nanosheets and PVA polymer.

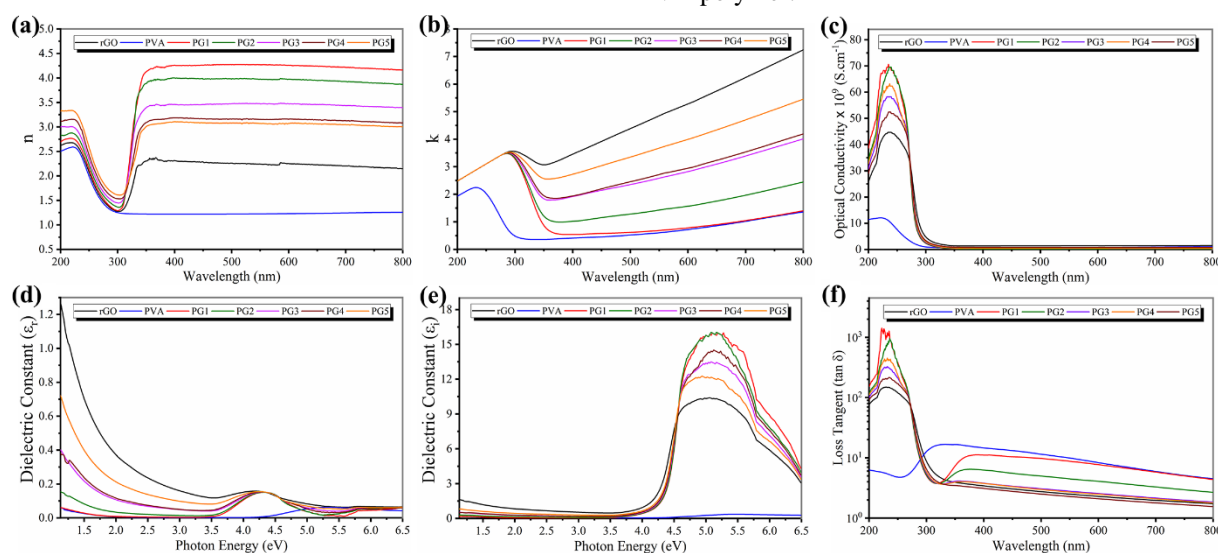


Figure 5. (a) the refractive index, (b) the extinction coefficient, (c) the optical conductivity, (d) and (e) the optical dielectric constant real (ϵ_r) and imaginary (ϵ_i) parts, respectively, and (f).

Conclusion

This study presents a detailed examination of the optical, structural, and dielectric properties of rGO-doped PVA nanocomposites. The comprehensive analysis of optical transparency and band structure parameters across varying rGO concentrations within the PVA matrix reveals significant insights. Our findings demonstrate a clear dependence of the optical bandgap, refractive index, optical dielectric constants, and optical conductivity on the rGO content. Understanding these mechanisms provides a foundation for developing more efficient and cost-effective materials for a broad spectrum of optical devices. As research continues, rGO-doped PVA nanocomposites are poised to make significant contributions to the advancement of flexible electronics, smart sensors, and next-generation photonic devices, underscoring their potential in future technological innovations.

Acknowledgements

The authors would like to acknowledge [RES Laboratory](#), Department of Physics, College of Sciences, Mustansiriyah University, Baghdad, Iraq.

Declaration of Competing Interests

The authors declare that they have no conflicts of interest.

References

- [1] M. Sarno, D. Scarpa, A. Senatore, and W. Ahmed Abdalgilil Mustafa, "rGO/GO Nanosheets in Tribology: From the State of the Art to the Future Prospective," *Lubricants*, vol. 8, no. 3, p. 20 <https://doi.org/10.3390/lubricants8030031>
- [2] N. Devi, R. Kumar, S. Singh, and R. K. Singh, "Recent development of graphene-based composite for multifunctional applications: energy, environmental and biomedical sciences," *Critical Reviews in Solid State and Materials Sciences*, vol. 49, no. 1, p. 72-140, 2024. <https://doi.org/10.1080/10408436.2022.2132910>.
- [3] R. M. Hameed, A. Al-Haddad, and A. K. Albarazanchi, "Influence of Graphene Sheets Accumulation on Optical Band Gap Enhanced Graphite Exfoliation," *Al-Mustansiriyah Journal of Science*, vol. 33, no. 4, p. 168-174, 2022. <http://doi.org/10.23851/mjs.v33i4.1216>.
- [4] R. M. Hameed, A. Al-Haddad, and A. K. Albarazanchi, "Facile transformation of graphene oxide nanospheres based on AAO template," *Kuwait Journal of Science*, vol. 50, no. 4, p. 563-568, 2023. <https://doi.org/10.1016/j.kjs.2023.08.002>.
- [5] B. L. Barroso *et al.*, "Enhanced mechanical and antimicrobial properties of hydroxypropyl methylcellulose films incorporating silver nanoparticles for wound dressing applications," *Polymer Bulletin*, 2024. <https://doi.org/10.1007/s00289-024-05217-w>.

- [6] T. N. Ghosh, S. S. Pradhan, S. K. Sarkar, and A. K. Bhunia, "On the incorporation of the various reduced graphene oxide into poly(vinyl alcohol) nanocompositions: comparative study of the optical, structural properties and magnetodielectric effect," *Journal of Materials Science - Materials in Electronics*, vol. 32, no. 14, p. 19157-19178, 2021.
<https://doi.org/10.1007/s10854-021-06435-y>.
- [7] U. E. Ruman *et al.*, "Biogenic-ecofriendly synthesized SnO₂/CuO/FeO/PVP/RGO nanocomposite for enhancing energy density performance of hybrid supercapacitors," *Journal of Energy Storage*, vol. 89, p. 111643, 2024.
<https://doi.org/10.1016/j.est.2024.111643>.
- [8] R. Gholipur, "Synthesis and characterization of novel PVA/MF-PC/RGO nanocomposites," *Diamond and Related Materials*, vol. 138, p. 110244, 2023.
<https://doi.org/10.1016/j.diamond.2023.110244>.
- [9] S. Yan, S. Xu, Y. Wang, J. You, C. Guo, and X. Wu, "A Hydrogel Dressing Comprised of Silk Fibroin, Ag Nanoparticles, and Reduced Graphene Oxide for NIR Photothermal-Enhanced Antibacterial Efficiency and Skin Regeneration," *Advanced Healthcare Materials*, p. 2400884, 2024.
<https://doi.org/10.1002/adhm.202400884>.
- [10] T. A. Hamdalla and T. A. Hanafy, "Optical properties studies for PVA/Gd, La, Er or Y chlorides based on structural modification," *Optik*, vol. 127, no. 2, p. 878-882, 2016.
<https://doi.org/10.1016/j.ijleo.2015.10.187>.
- [11] S. Stankovich *et al.*, "Synthesis of graphene-based nanosheets via chemical reduction of exfoliated graphite oxide," *Carbon*, vol. 45, no. 7, p. 1558-1565, 2007.
<https://doi.org/10.1016/j.carbon.2007.02.034>.
- [12] M. Fang, K. Wang, H. Lu, Y. Yang, and S. Nutt, "Single-layer graphene nanosheets with controlled grafting of polymer chains," *Journal of Materials Chemistry*, vol. 20, no. 10, p. 1982-1992, 2010.
<https://doi.org/10.1039/B919078C>.
- [13] S. K. Marka, B. Sindam, K. C. James Raju, and V. V. S. S. Srikanth, "Flexible few-layered graphene/poly vinyl alcohol composite sheets: synthesis, characterization and EMI shielding in X-band through the absorption mechanism," *RSC Advances*, vol. 5, no. 46, p. 36498-36506, 2015.
<https://doi.org/10.1039/C5RA04038H>.
- [14] W. Liu and G. Speranza, "Tuning the Oxygen Content of Reduced Graphene Oxide and Effects on Its Properties," *ACS Omega*, vol. 6, no. 9, p. 6195-6205, 2021.
<https://doi.org/10.1021/acsomega.0c05578>.
- [15] Y. y. Wang *et al.*, "Raman Studies of Monolayer Graphene: The Substrate Effect," *The Journal of Physical Chemistry C*, vol. 112, no. 29, p. 10637-10640, 2008.
<https://doi.org/10.1021/jp8008404>.
- [16] J. Cao *et al.*, "High-strength graphene composite films by molecular level couplings for flexible supercapacitors with high volumetric capacitance," *Journal of Materials Chemistry A*, vol. 5, no. 29, p. 15008-15016, 2017.
<https://doi.org/10.1039/C7TA04920J>.
- [17] M. Sharma, S. Rani, D. K. Pathak, R. Bhatia, R. Kumar, and I. Sameera, "Temperature dependent Raman modes of reduced graphene oxide: Effect of anharmonicity, crystallite size and defects," *Carbon*, vol. 184, p. 437-444, 2021.
<https://doi.org/10.1016/j.carbon.2021.08.014>.
- [18] D. Bhatnagar, S. Singh, S. Yadav, A. Kumar, and I. Kaur, "Experimental and theoretical investigation of relative optical band gaps in graphene generations," *Materials Research Express*, vol. 4, no. 1, p. 015101, 2017.
<https://doi.org/10.1088/2053-1591/4/1/015101>.
- [19] X. Yang, L. Li, S. Shang, and X.-m. Tao, "Synthesis and characterization of layer-aligned poly(vinyl alcohol)/graphene nanocomposites," *Polymer*, vol. 51, no. 15, p. 3431-3435, 2010.
<https://doi.org/10.1016/j.polymer.2010.05.034>.
- [20] S. Gahlot, P. P. Sharma, V. Kulshrestha, and P. K. Jha, "SGO/SPES-Based Highly Conducting Polymer Electrolyte Membranes for Fuel Cell Application," *ACS Applied Materials & Interfaces*, vol. 6, no. 8, p. 5595-5601, 2014.
<https://doi.org/10.1021/am5000504>.
- [21] C. Bao, Y. Guo, L. Song, and Y. Hu, "Poly(vinyl alcohol) nanocomposites based on graphene and graphite oxide: a comparative investigation of property and mechanism," *Journal of Materials Chemistry*, vol. 21, no. 36, p. 13942-13950, 2011.
<https://doi.org/10.1039/C1JM11662B>.
- [22] L. Lu, H. Sun, F. Peng, and Z. Jiang, "Novel graphite-filled PVA/CS hybrid membrane for pervaporation of benzene/cyclohexane mixtures," *Journal of Membrane Science*, vol. 281, no. 1, p. 245-252, 2006.
<https://doi.org/10.1016/j.memsci.2006.03.041>.
- [23] Y. Chen, X. Zhang, P. Yu, and Y. Ma, "Stable dispersions of graphene and highly conducting graphene films: a new approach to creating colloids of graphene monolayers," *Chemical Communications*, no. 30, p. 4527-4529, 2009.
<https://doi.org/10.1039/B907723E>.
- [24] Y. Xu, W. Hong, H. Bai, C. Li, and G. Shi, "Strong and ductile poly(vinyl alcohol)/graphene oxide composite films with a layered structure," *Carbon*, vol. 47, no. 15, p. 3538-3543, 2009.
<https://doi.org/10.1016/j.carbon.2009.08.022>.
- [25] H. Chen *et al.*, "Citrate-based fluorophores in polymeric matrix by easy and green in situ synthesis for full-band UV shielding and emissive transparent display," *Journal of Materials Science*, vol. 54, no. 2, p. 1236-1247, 2019.
<https://doi.org/10.1007/s10853-018-2933-9>.
- [26] H. K. F. Cheng *et al.*, "Poly(vinyl alcohol) Nanocomposites Filled with Poly(vinyl alcohol)-Grafted Graphene Oxide," *ACS Applied Materials & Interfaces*, vol. 4, no. 5, p. 2387-2394, 2012.
<https://doi.org/10.1021/am300550n>.
- [27] L. Bi *et al.*, "Structural, magnetic, and optical properties of BiFeO₃ and Bi₂FeMnO₆ epitaxial thin films: An experimental and first-principles study," *Physical Review B*, vol. 78, no. 10, p. 104106, 2008.

<https://doi.org/10.1103/PhysRevB.78.104106>.

[28] T. N. Ghosh, A. K. Bhunia, S. S. Pradhan, and S. K. Sarkar, "Electric modulus approach to the analysis of electric relaxation and magnetodielectric effect in reduced graphene oxide–poly(vinyl alcohol) nanocomposite," *Journal of Materials Science - Materials in Electronics*, vol. 31, no. 18, p. 15919-15930, 2020.

<https://doi.org/10.1007/s10854-020-04153-5>.

[29] A. K. Bhunia and S. Saha, "Characterization of budding twigs of flower-type zinc oxide nanocrystals for the fabrication and study of nano-ZnO/p-Si heterojunction UV light photodiode," *Journal of Materials Science - Materials in Electronics*, vol. 32, no. 8, p. 9912-9928, 2021.

<https://doi.org/10.1007/s10854-021-05649-4>.

[30] M. Yass, A. Al-Haddad, and A. J. Sadeq, "Optical and Degradation Characteristics of Green Synthesized Cornstarch-Base Bioorganic Polymer," (in en), *Al-Mustansiriyah Journal of Science*, vol. 35, no. 1, p. 95-103, 2024.

<https://doi.org/10.23851/mjs.v35i1.1404>.

[31] R. M. Abdullah, S. B. Aziz, S. M. Mamand, A. Q. Hassan, S. A. Hussein, and M. F. Z. Kadir, "Reducing the Crystallite Size of Spherulites in PEO-Based Polymer Nanocomposites Mediated by Carbon Nanodots and Ag Nanoparticles," *Nanomaterials*, vol. 9, no. 6, p. 874, 2019.

<https://doi.org/10.3390/nano9060874>.